

# Progressive Choriocapillaris Impairment in *ABCA4* Maculopathy Is Secondary to Retinal Pigment Epithelium Atrophy

Ruben Jauregui,<sup>2,3</sup> Ahra Cho,<sup>1,2,4</sup> Winston Lee,<sup>1</sup> Jana Zernant,<sup>1</sup> Rando Allikmets,<sup>1,5</sup> Janet R. Sparrow,<sup>1,2,5</sup> and Stephen H. Tsang<sup>1,2,5</sup>

<sup>1</sup>Department of Ophthalmology, Edward S. Harkness Eye Institute, Columbia University Medical Center, New York, United States

<sup>2</sup>Jonas Children's Vision Care and Bernard and Shirlee Brown Glaucoma Laboratory, New York, United States

<sup>3</sup>Weill Cornell Medical College, New York, United States

<sup>4</sup>Institute of Human Nutrition, College of Physicians and Surgeons, Columbia University, New York, United States

<sup>5</sup>Department of Pathology and Cell Biology, Columbia University Medical Center, New York, United States

Correspondence: Stephen H. Tsang, Harkness Eye Institute, Columbia University Medical Center, 635 West 165th Street, Box 212, New York, NY 10032, USA;

sht2@cumc.columbia.edu.

Received: January 4, 2020

Accepted: February 3, 2020

Published: April 16, 2020

Citation: Jauregui R, Cho A, Lee W, et al. Progressive choriocapillaris impairment in *ABCA4* maculopathy is secondary to retinal pigment epithelium atrophy. *Invest Ophthalmol Vis Sci.* 2020;61(4):13. <https://doi.org/10.1167/iovs.61.4.13>

**PURPOSE.** To analyze the progression of choriocapillaris (CC) impairment in recessive Stargardt disease (STGD) and compare it to the progression of retinal pigment epithelium (RPE) atrophy.

**METHODS.** Fifty-five patients with a clinical diagnosis of STGD and genetic confirmation of pathogenic biallelic variants in *ABCA4* were imaged with short-wavelength fundus autofluorescence (SW-AF) and optical coherence tomography angiography (OCTA) at a single clinic visit, whereas a subset of 12 patients were imaged with the same modalities at two different clinic visits.

**RESULTS.** We observed three stages of CC impairment: an area of bright yet intact macular CC (11 patients), regions of vascular rarefaction and incomplete CC atrophy within an area of bright CC (10 patients), and areas of extensive CC atrophy (26 patients). These changes correlated to the degree of RPE atrophy observed in SW-AF imaging. Furthermore, 8 patients presented with early changes on SW-AF, but healthy CC. Quantitative analyses of the atrophic changes revealed that the area of RPE atrophy is larger ( $9.6 \pm 1.7 \text{ mm}^2$  vs.  $6.9 \pm 1.3 \text{ mm}^2$ ,  $P < 0.001$ ) and that it progresses at a faster rate ( $1.1 \pm 0.1 \text{ mm}^2/\text{year}$  vs.  $0.8 \pm 0.2 \text{ mm}^2/\text{year}$ ,  $P = 0.004$ ) than the corresponding area of CC atrophy.

**CONCLUSIONS.** CC impairment is progressive and OCTA imaging can be used to demonstrate the stages, which culminate in extensive CC atrophy. Furthermore, CC impairment is secondary to RPE atrophy in STGD. We further advocate the use of SW-AF and OCTA imaging in monitoring the progression of STGD.

Keywords: Stargardt, optical coherence tomography angiography, retinal pigment epithelium, choriocapillaris

Recessive Stargardt disease (STGD; OMIM: 248200) is inherited in an autosomal recessive manner and is caused by mutations in the *ABCA4* gene, which codes for the photoreceptor-specific adenosine triphosphatase (ATP)-binding cassette transporter and was first identified as causative in 1997.<sup>1</sup> With an estimated prevalence of 1 in 10,000, STGD is the most common retinal dystrophy with over 1000 pathogenic variants identified to date.<sup>1-3</sup> The typical presentation involves yellow, pisciform flecks along with macular atrophy that leads to central vision loss.<sup>3-5</sup> Nevertheless, STGD exhibits extensive clinical heterogeneity, readily apparent in fundus imaging and presentation. For example, patients can present with disease onset early in adulthood (adult-onset) or late in adulthood (late-onset), both of which are usually associated with milder disease, whereas early-onset (early or before teenage years) is associated with more severe disease.<sup>4,6-8</sup>

Imaging of the posterior pole has become an essential tool for the clinician in the diagnosis and monitoring of retinal dystrophies, including STGD. Short-wavelength fundus autofluorescence (SW-AF) is an important imaging modality for STGD, as the areas of retinal pigment epithelium (RPE) atrophy that characterize the disease are readily observed as areas of hypofluorescence.<sup>9,10</sup> Recently, optical coherence tomography angiography (OCTA) has been increasingly used to analyze the retinal and choroidal vasculatures in the study of retinal dystrophies.<sup>5,11-15</sup> OCTA uses streaming blood flow to create an image showing the retinal vasculature. Individual choriocapillaris (CC) vessels are not visualized, but rather appear as homogeneous with areas of brightness representing blood flow.<sup>16</sup> As compared with fluorescein (FA) and indocyanine green angiography (ICGA), the gold standard for evaluating the retinal and choroidal vasculature, respectively, OCTA is

a noninvasive imaging modality that provides faster and high-resolution imaging, avoiding the use of a dye and its potential complications.<sup>17,18</sup> Furthermore, FA and ICGA are not able to image the deep layers of vasculature well, such as the deep capillary plexuses or CC, whereas OCTA can provide high-contrast imaging of these layers.<sup>17,18</sup>

In this study, we evaluated the stages of CC atrophy in STGD and compared them to the progression of RPE impairment by using both OCTA and SW-AF imaging.

## METHODS

### Patients

This study is adherent to the tenets of the Declaration of Helsinki. The study procedures were defined, and patient consent obtained as outlined by the protocol #AAAI9906 approved by the institutional review board at Columbia University Medical Center. None of the data presented in this study are identifiable to individual patients, including genetic testing results and imaging. We conducted a retrospective review of patients with a diagnosis of STGD at the Harkness Eye Institute. The clinical diagnosis was made by a retinal dystrophies specialist (SHT) based on presenting symptoms, clinical imaging, and/or genetic testing. The inclusion criteria for this study were the diagnosis of STGD confirmed by genetic testing (two pathogenic variants in *ABCA4*) and at least one visit to our clinic during which SW-AF and OCTA imaging were both obtained. Exclusion criteria precluded those patients without SW-AF or OCTA imaging or those whose lesion size extended beyond the area of image capture by either modality (55° field of view for SW-AF and 8 × 8 mm for OCTA). Furthermore, retinal disease caused by other genes, such as *CRX* and *PRPH2*, can phenotypically mimic STGD.<sup>19</sup> Thus given that unequivocal diagnosis of STGD is established when biallelic variants in *ABCA4* are documented, patients with only a single identified possibly pathogenic variant were excluded from this study. A total of 55 patients qualified for this study from our patient registry.

### Clinical Examination

Each patient underwent a full ophthalmic examination, including a slit-lamp and dilated funduscopic examination, spectral-domain optical coherence tomography (SD-OCT), SW-AF (488 nm excitation), and OCTA. Examination and imaging across all modalities were conducted after pupillary dilation (>7 mm) with phenylephrine hydrochloride (2.5%) and tropicamide (1%). SW-AF images were acquired with the Spectralis HRA+OCT (Heidelberg Engineering, Heidelberg, Germany), whereas OCTA images were acquired using the Zeiss AngioPlex Cirrus HD-OCT 5000 (Zeiss Meditec, Inc., Dublin, CA, USA). Images of the CC via OCTA were obtained by automated segmentation of full-thickness retina scans into different vascular layers performed by the OCTA machine.

### Image and Statistical Analyses

The OCTA images for each of the 55 patients were analyzed by two independent graders (RJ and AC). A subset of 26 patients presented with well-demarcated areas of CC atrophy on OCTA imaging. These patients were further analyzed quantitatively by measuring these areas of CC atrophy and comparing them to the areas of RPE atrophy in

SW-AF imaging. Both eyes of each patient were analyzed. Measurements of RPE atrophy on SW-AF images were performed using the built-in measurement tool in the Spectralis HRA+OCT software, whereas CC atrophy on OCTA imaging was measured by using the software ImageJ 1.8.0 (National Institutes of Health, Bethesda, MD, USA).<sup>20</sup> The same SW-AF/OCTA image was analyzed twice by two independent graders (RJ and AC) to mitigate bias and error in measurement. The Pearson correlation was used to analyze the measurement agreement by the two graders (SW-AF:  $r = 0.999$ ,  $P < 0.001$ ; OCTA:  $r = 0.999$ ,  $P < 0.001$ ). Furthermore, Bland-Altman analyses were performed to further characterize measurement agreement and reproducibility (Supplementary Fig. S1). Given the high level of correlation and agreement of the measurements between the two graders, the average of the two values was calculated and used for subsequent analyses. A paired Student's *t*-test was used to test for a difference in the size of RPE and CC atrophy between SW-AF and OCTA imaging, respectively. From this subset of patients, 12 presented at 2 separate clinic visits in which both sets of images were acquired and analyses of disease progression were performed. The rate of progression, defined as the difference in lesion size between the first and subsequent visit divided by the length of follow-up, was calculated for each imaging modality. The statistical analyses were performed using the Stata 12.1 software (StataCorp, College Station, TX, USA). Bland-Altman plots and analyses were performed using GraphPad Prism 8 software (GraphPad Software, San Diego, CA, USA).

## RESULTS

Fifty-five patients with genetically confirmed STGD were included in the study. The average age of the cohort was  $35 \pm 18$  years (mean  $\pm$  SD). Genetic screening identified biallelic variants for all patients (Supplementary Table S1). In addition to normal CC, we observed three different phenotypes of CC on OCTA imaging: an area of bright yet intact macular CC, regions of vascular rarefaction and incomplete CC atrophy in an area of bright macular CC, and areas of extensive CC atrophy.

Eight patients (15%) included in group 1 presented with no lesions on OCTA imaging. Instead the CC were homogeneous in appearance, similar to healthy subjects (Fig. 1). When analyzing the SW-AF images, minimal changes were observed. All these patients exhibited a small, nascent region of macular hypoautofluorescence (hypoAF), with a surrounding ring of hyperautofluorescence (hyperAF), resembling a bull's eye phenotype. Fundoscopy on these patients was unremarkable. One patient presented with yellow flecks on funduscopy, which were hyperAF on SW-AF, but nascent macular hypoAF and healthy CC were also present (Fig. 1D).

Eleven patients (20%) included in group 2 presented with an area of homogeneous yet bright CC in association with the macula (Figs. 2A–D), whereas 10 patients (18%) in group 3 presented with regions of vascular rarefaction and incomplete atrophy within the area of bright macular CC (Figs. 2E–H). All patients in both groups presented with obvious macular RPE atrophy, observed as hypoAF areas on SW-AF. Nevertheless, within both groups the degree of macular RPE atrophy varied and ranged from mild to moderate hypoAF.

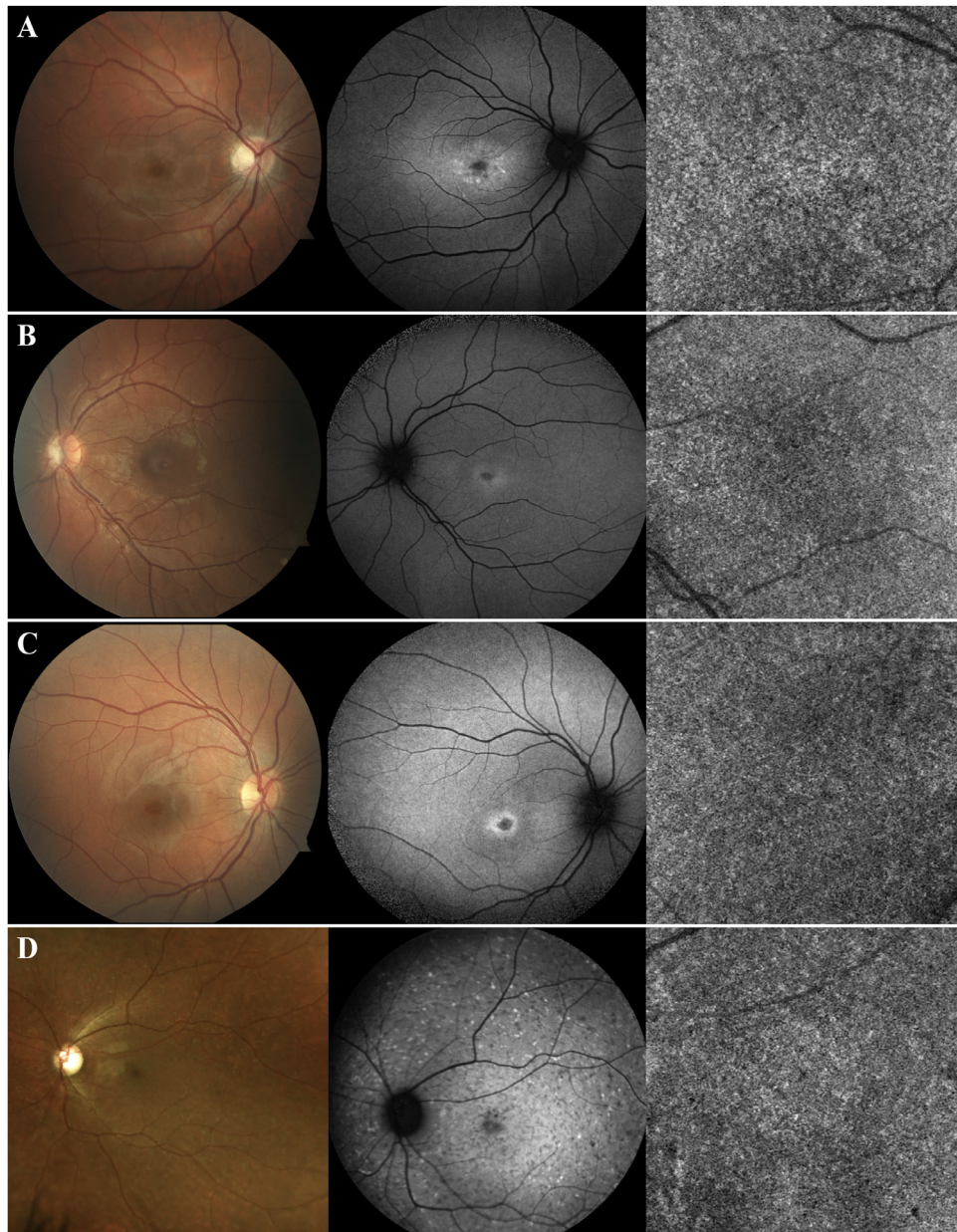


**FIGURE 1.** Patients with early changes on SW-AF due to recessive STGD but healthy CC (group 1). Color fundus photography, SW-AF, and OCTA imaging of patients **A–D**. These patients present with a small area of macular hypoAF with a surrounding ring of hyperAF, both early changes associated with recessive STGD. Nevertheless, the CC appear healthy with no changes on OCTA imaging. Fundoscopy is unremarkable for patients **A–C**. For patient **D**, hyperAF flecks on SW-AF and *yellow flecks* on funduscopy are observed, both characteristic of STGD.

Finally, 26 patients (47%) comprised group 4 and presented with areas of demarcated CC atrophy (Fig. 3). In these patients, the underlying larger choroidal vessels were visualized owing to the disappearance of the overlying CC. In SW-AF images, these areas appeared as severe, dense, well-demarcated, hypoAF areas that suggest extensive RPE atrophy. On SD-OCT images, increased signal transmission into the choroid was observed in these areas along with the loss of the outer retinal layers and subsequent collapse of the inner retinal layers. On funduscopy, the underlying white sclera was visible in these areas of RPE and CC atrophy.

Because the areas of RPE and CC atrophy were well demarcated for this last group of 26 patients (52 eyes),

we analyzed quantitatively the size of the impairments in both imaging modalities and compared them (Fig. 4). We observed that size of the areas of RPE atrophy,  $8.2 \pm 1.5 \text{ mm}^2$  (mean  $\pm$  SE), was larger than those of CC atrophy,  $5.9 \pm 1.2 \text{ mm}^2$  ( $P < 0.001$ ). This was observed for all 26 patients. From this subgroup, both SW-AF and OCTA were acquired at two separate clinic visits for 12 patients (24 eyes) and we calculated the rate of progression for RPE and CC atrophy. The average follow-up time between the two visits was  $1.2 \pm 0.8$  years. We observed that the area of RPE atrophy increased in size at a faster rate,  $1.1 \pm 0.2 \text{ mm}^2/\text{year}$ , as compared with the area of CC impairment,  $0.8 \pm 0.2 \text{ mm}^2/\text{year}$  ( $P = 0.005$ ). These results are summarized in the Table.

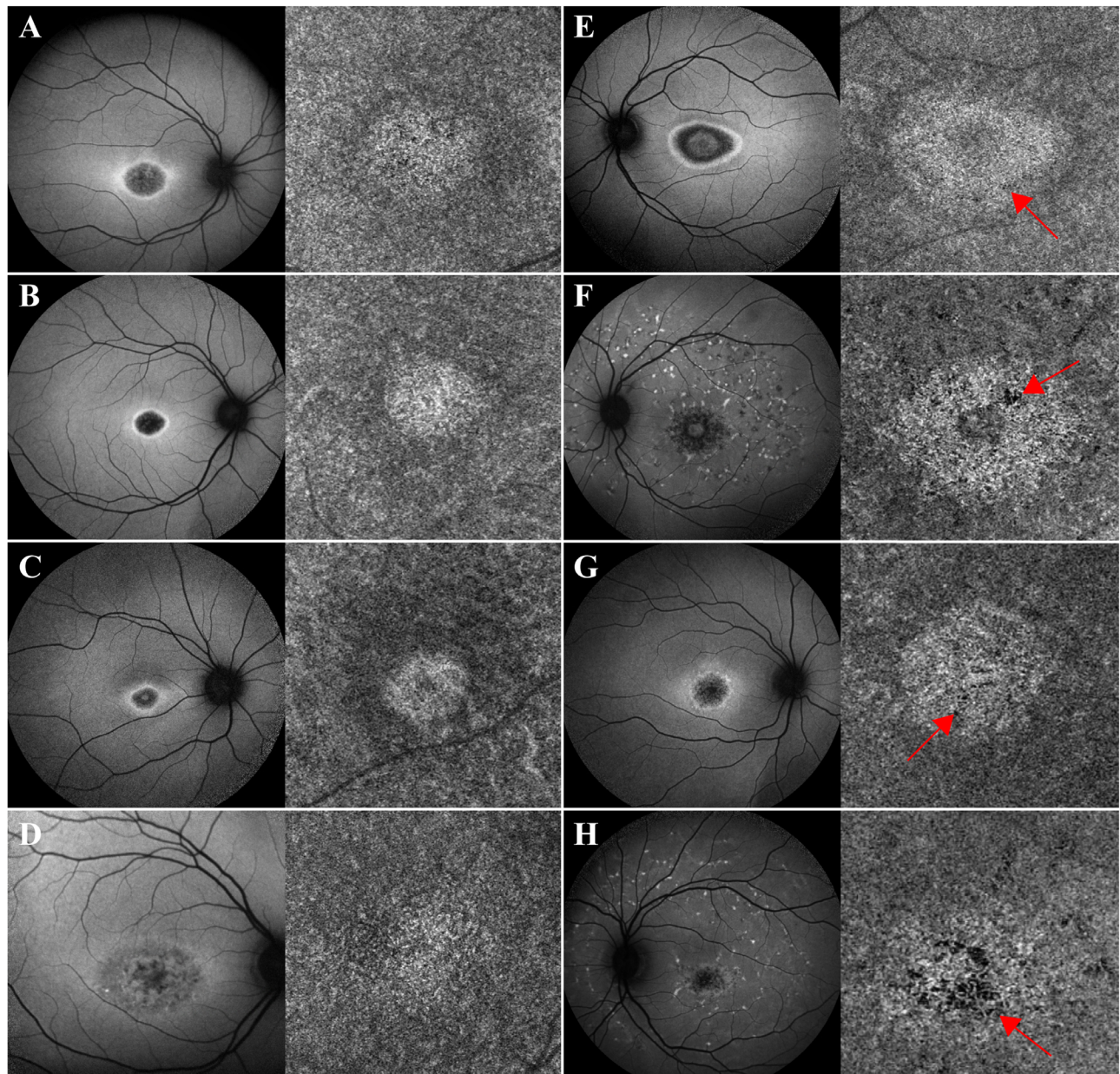


**FIGURE 2.** Patients with STGD exhibiting an area of bright macular CC (groups 2 and 3). Patients **A–D** presented with an area of bright macular yet intact CC on OCTA corresponding to the area of macular atrophy observed in SW-AF imaging. Despite the overlying RPE atrophy, the CC appear intact (group 2). Patients **E–H** also presented with an area of bright macular CC, but in these patients, there is obvious vascular rarefaction and CC atrophy (*red arrows*) (group 3). The CC changes observed in both groups of patients correspond to the overlying RPE atrophy, although damage in group 3 patients is more advanced.

**TABLE.** Comparison of the Size of RPE and CC Atrophy as Measured with SW-AF and OCTA Imaging in Patients with a Single Visit, and the Progression Rate of These Areas of Atrophy in Patients with Two Visits

Imaging Modality	Single Visit			Two Visits			
	N	Size of Atrophy (mm <sup>2</sup> )	P value*	N	Follow-Up Time (y)	Progression Rate (mm <sup>2</sup> /y)	P value*
SW-AF	52	8.2 ± 1.5 mm <sup>2</sup>	< 0.001	24	1.2 ± 0.8	1.1 ± 0.2	0.005
OCTA		5.9 ± 1.2 mm <sup>2</sup>				0.8 ± 0.2	

Data are summarized as mean ± SE for the size of atrophy and progression rates, whereas mean ± SD is used for the follow-up times. N, number of eyes analyzed.

\* Calculated using a paired Student's *t*-test.

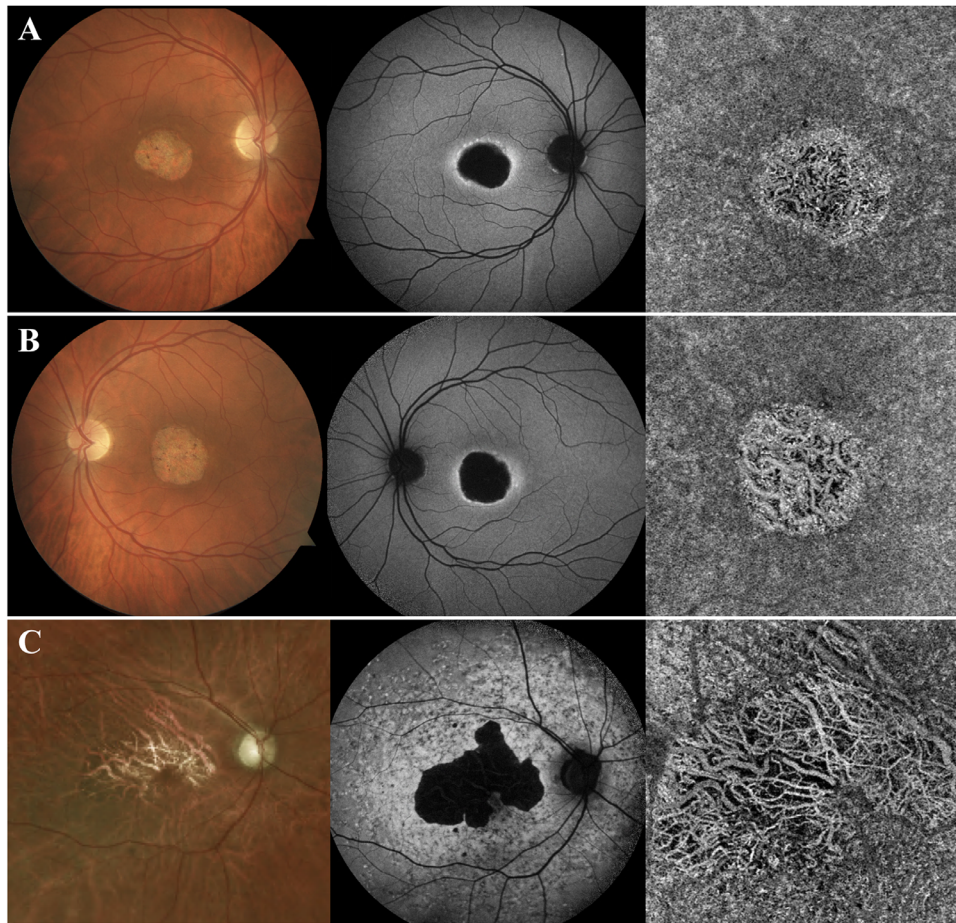


**FIGURE 3.** Patients with STGD with extensive CC atrophy in areas of retinal atrophy (group 4). Patients A–C presented with extensive atrophy of the CC, with visualization of the underlying larger choroidal vessels. These areas of atrophy corresponded to areas of extensive RPE loss on SW-AF imaging, as suggested by the dense areas of hypoAF. Furthermore, the underlying *white sclera* was visible on funduscopy on these areas.

## DISCUSSION

Previous studies reported blood flow abnormalities in retinal dystrophies by using a variety of imaging modalities, such as magnetic resonance imaging.<sup>21–24</sup> Currently, OCTA has become the primary modality to analyze the retinal and choroidal vasculature in a variety of retinal dystrophies, including retinitis pigmentosa, choroideremia, and STGD.<sup>5,11–15,25</sup> In STGD, studies by Mastropasqua et al.<sup>12</sup> and Battaglia Parodi et al.<sup>13</sup> reported vascular impairments at the levels of the superficial capillary, deep capillary plexus, and CC. Furthermore, Alabduljalil et al.<sup>5</sup> reported a strong correlation between the area of RPE atrophy on SW-AF imaging and loss of the inner and outer segment junction on SD-OCT, concluding that photoreceptor degeneration precedes RPE atrophy. A smaller study by de Carlo et al.<sup>14</sup> examined seven patients with retinal dystrophies, including four with STGD, and concluded that because CC changes were smaller than the corresponding RPE alterations, vascular loss is a secondary process. Despite the insights offered by these studies, we were further interested in exploring the progression of CC and RPE atrophy in a large cohort of genetically confirmed STGD.

Analyses of the OCTA images from our patient cohort revealed four different phenotypes of CC. In addition to

normal CC (group 1 patients), we observed two phenotypes with bright macular CC, suggesting apparent increased blood flow: one with homogeneous CC (group 2 patients), and another with vascular rarefaction and incomplete CC atrophy (group 3 patients). Nevertheless, as suggested in a previous study, our view is that the CC brightness is not owing to an increase in blood flow but is rather an artifact because of the disappearance of the overlying RPE because as it atrophies more signal is received in that area as compared with the regions with the intact overlying RPE.<sup>12</sup> All the patients with bright macular CC have corresponding RPE atrophy as indicated by SW-AF images (Fig. 2). We also observed that around the perimeter of the lesion, there is a dark halo that extends outward in a nonspecific manner (Fig. 5). We believe that this halo is a shadow cast by lipofuscin accumulation in the RPE overlying the CC, in a similar yet opposite manner as to how the CC appear bright when the overlying RPE atrophies. This is further supported by analyzing the SW-AF images of patients with hyper-AF flecks, as these seem to cast dark spots on the underlying CC (Fig. 5). Thus OCTA imaging not only plays a role in demonstrating CC atrophy, but also in indirectly showing the accumulation of lipofuscin in the overlying RPE. The pathophysiology of STGD involves defective transport of all-trans-retinal, leading to the accentuated

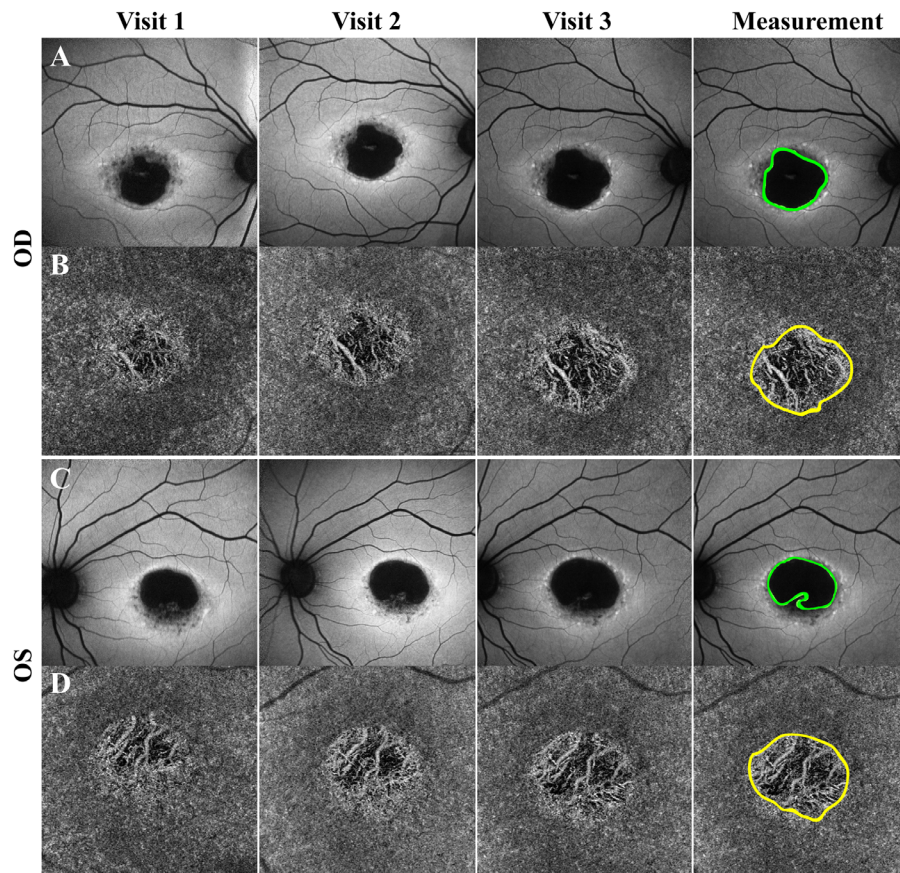


**FIGURE 4.** Progressive atrophy detected in SW-AF and OCTA imaging of patients with STGD. SW-AF (A, C) and OCTA (B, D) of a patient with three clinical visits each 1 year apart. As observed on SW-AF, the area of hypoAF increases in size between the visits, suggesting progressive atrophy of the RPE. Similarly, progression of CC atrophy is observed on OCTA imaging as indicated by the increased area of atrophy and greater visualization of the underlying choroidal vessels. The last panel shows the areas of atrophy being outlined to analyze and compare the size of RPE versus CC atrophy quantitatively. OS, oculus sinister; OD, oculus dextrus.

production of bisretinoids, which are photoreactive and toxic to the RPE and photoreceptor cells and cause their eventual death.<sup>6,10,26,27</sup> The last observed phenotype demonstrated extensive RPE and CC atrophy, often with the larger choroidal vessels visible (patients in group 4).

We believe that these phenotypes are snapshots of the disease continuum and represent different stages of STGD-associated CC impairment, with the rate of atrophy determined by the patient's genotype. The disease course involves a progressive atrophy of the RPE. As the overlying RPE atrophies, the underlying CC appear brighter than the rest of the CC, with progressive impairment leading to vascular rarefaction and incomplete CC atrophy. Finally, the process ends with extensive atrophy of the CC in which the larger choroidal vessels become visible. The disappearance of CC and increase in the area of CC atrophy are evident in the imaging of the patients with multiple clinic visits (Fig. 4). Furthermore, analyses of the patients' genotypes revealed that 24 patients (44%) presented with the G1961E variant (one patient was homozygous, the rest were compound heterozygotes). When we segregate by groups, group 1 contained the highest proportion of patients with a G1961E allele (75%), whereas groups 2 through 4 contained 45%, 40%, and 31%, respectively. Given that patients in group 1 presented with no changes on OCTA and mild changes in SW-AF imaging, our genotype analysis suggests that the

G1961E allele is associated with milder disease severity, which has been previously reported by other studies from our group.<sup>28–30</sup> Future studies of larger patient cohorts should further characterize the relationship between vasculature changes in OCTA and a patient's genotype.

Similar to the aforementioned studies, our results suggest that CC atrophy is secondary to RPE impairments in STGD. Given the well-demarcated areas on patients with extensive RPE and CC atrophy, we were able to measure the size of the impairment and compare it to each other. With this quantitative analysis, we observed that the area of RPE atrophy is larger than that of CC atrophy (9.6 vs. 6.9 mm<sup>2</sup>,  $P < 0.001$ ), whereas we also observed that the area of RPE atrophy progresses at a faster rate than that of CC atrophy (1.1 vs. 0.8 mm<sup>2</sup>/year,  $P = 0.005$ ). In addition, we observed a group of eight patients with early changes in SW-AF but healthy CC, further supporting our claim that RPE damage occurs before CC impairment. The RPE plays a critical role in the support of the CC by generating vascular endothelial growth factor, a cytokine important for the development and maintenance of the CC.<sup>31,32</sup> We believe that as the RPE atrophies, the disappearance of the CC follows as a downstream effect.

We use SW-AF imaging to discuss progressive RPE atrophy in STGD in relation to CC as shown by OCTA. Another commonly used imaging modality used to study the state of RPE is near-infrared autofluorescence (NIR-AF) imaging

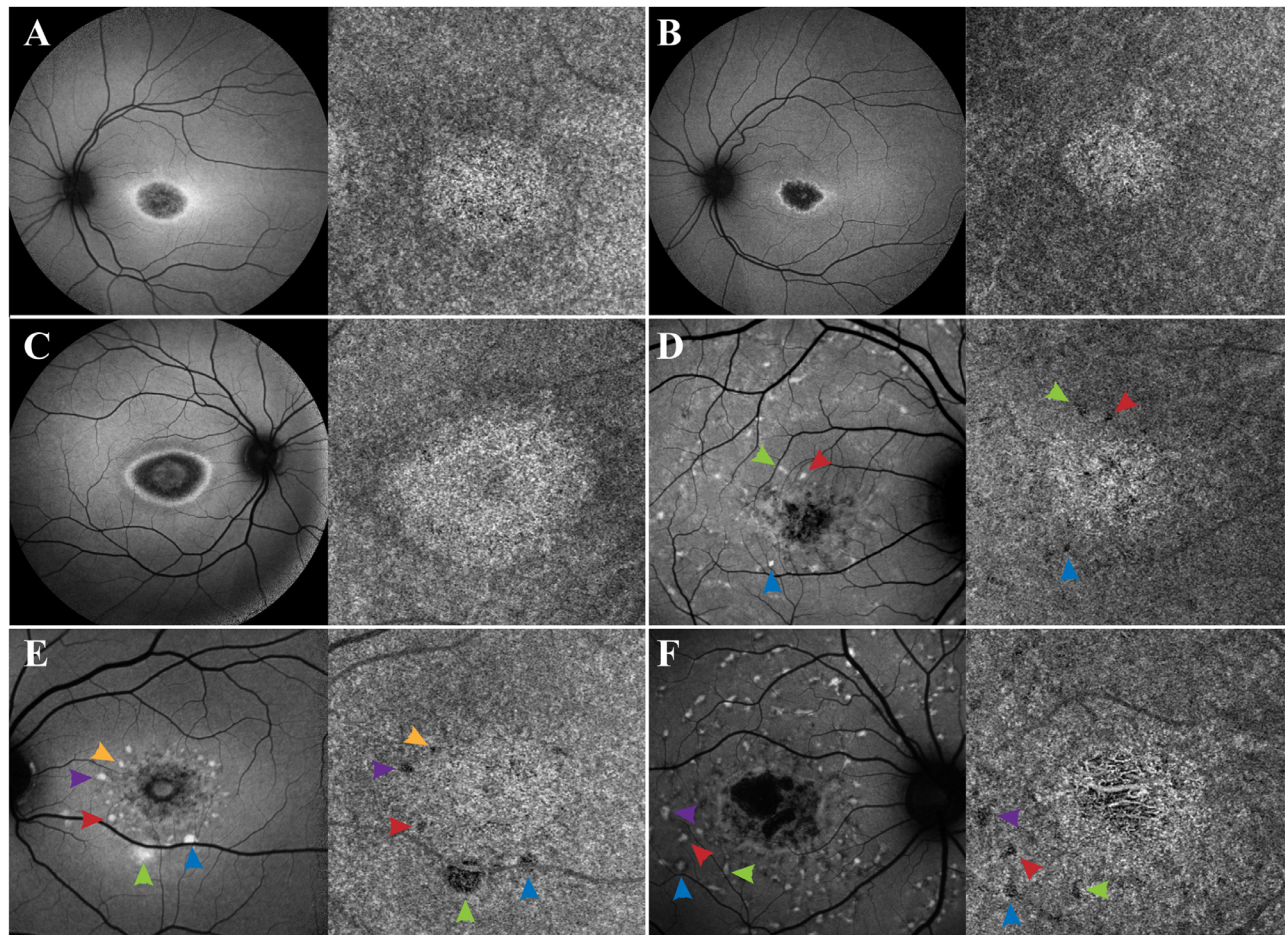


**FIGURE 5.** Accumulation of lipofuscin in the overlying RPE creates a shadow on the underlying CC. In patients **A–F**, SW-AF reveals variable degrees of macular RPE atrophy, with the lesion appearing bright on the underlying CC as observed on OCTA imaging. This apparent brightness of the lesion is likely created as more signal is received on this area owing to the atrophy of the overlying RPE. In addition, an apparent dark halo is appreciated on the perimeter surrounding the bright lesion on the CC. This shadow is likely created due to signal blockage from the lipofuscin that has accumulated on the overlying RPE, as appreciated from the hyperAF ring surrounding the macular atrophy on SW-AF imaging. The blockage of signal by RPE lipofuscin is further supported by analyzing the hyperAF flecks in patients **D–F**, as these flecks create a dark spot on the CC images (indicated by the matching color arrows on SW-AF and OCTA imaging).

(787 nm excitation), in which the signal comes from melanin in the RPE with a smaller contribution from the choroid.<sup>33</sup> Previous studies from our group have demonstrated that SW-AF underestimates the area of RPE atrophy in STGD.<sup>10,34</sup> Thus although we show that RPE atrophy is more extensive than CC atrophy, the degree of RPE atrophy might actually be more expansive if NIR-AF would have been used. The relationship between NIR-AF and OCTA imaging should be further explored.

Our study presents with some limitations. One is that patients with advanced disease could not be studied, as high-quality imaging is precluded by a lack of fixation. Furthermore, in our measurements of CC atrophy from the OCTA images, we did not correct for ocular magnification by accounting for axial length, as this measurement was not obtained during clinic visits.<sup>35–37</sup> This correction is important in young patients during eye growth. Nevertheless, of the 26 patients from whom we acquired measurements, only 3 (11%) were younger than age 20. Furthermore, because eye growth is associated with an increase in the absolute  $\mu\text{m}$  per pixel in the image scale, our measurements of CC lesion size are underestimated. This would suggest that the

difference between CC and RPE atrophy is actually larger than what we report, and further supports our conclusion that CC impairment is secondary to RPE atrophy.

## CONCLUSIONS

Our study shows that there is progressive impairment of the CC and eventual atrophy. Thus to avoid the added obstacle of impaired vasculature, therapeutic approaches that act on the RPE and/or photoreceptors should intervene at a stage in which there is minimal or no damage to the CC. We hope that our study brings awareness to the use of OCTA in identifying different stages of CC impairment in STGD, and further advocates the use of OCTA in monitoring the progression of STGD.

## Acknowledgments

Supported by the National Institutes of Health (Grants P30 EY019007, R01 EY024091, R01 EY018213, R01 EY024698, R01 EY026682, R01 EY028203, R01 EY028954, R01 EY029315, and R21 AG050437); National Cancer Institute Core 5P30CA013696;

Foundation Fighting Blindness awards TA-NMT-0116-0692-COLU and PPA-1218-0751-COLU; the Research to Prevent Blindness (RPB) Physician-Scientist Award, and the unrestricted grant to the Department of Ophthalmology, Columbia University, from RPB, New York, New York, United States. The authors alone are responsible for the content and writing of the article.

Disclosure: **R. Jauregui**, None; **A. Cho**, None; **W. Lee**, None; **J. Zernant**, None; **R. Allikmets**, None; **J.R. Sparrow**, None; **S.H. Tsang**, None

## References

- Allikmets R, Singh N, Sun H, et al. A photoreceptor cell-specific ATP-binding transporter gene (ABCR) is mutated in recessive Stargardt macular dystrophy. *Nat Genet.* 1997;15:236–246.
- Zernant J, Lee W, Collison FT, et al. Frequent hypomorphic alleles account for a significant fraction of ABCA4 disease and distinguish it from age-related macular degeneration. *J Med Genet.* 2017;54:404–412.
- Jauregui R, Cho GY, Takahashi VKL, et al. Caring for hereditary childhood retinal blindness. *Asia Pac J Ophthalmol (Phila).* 2018;7:183–191.
- Collison FT, Lee W, Fishman GA, et al. Clinical characterization of Stargardt disease patients with the p.N1868I ABCA4 mutation. *Retina.* 2019;39:2311–2325.
- Alabduljalil T, Patel RC, Alqahtani AA, et al. Correlation of outer retinal degeneration and choriocapillaris loss in Stargardt disease using en face optical coherence tomography and optical coherence tomography angiography. *Am J Ophthalmol.* 2019;202:79–90.
- Lambertus S, van Huet RA, Bax NM, et al. Early-onset Stargardt disease: phenotypic and genotypic characteristics. *Ophthalmology.* 2015;122:335–344.
- Westeneng-van Haften SC, Boon CJ, Cremers FP, Hoefsloot LH, den Hollander AI, Hoyng CB. Clinical and genetic characteristics of late-onset Stargardt's disease. *Ophthalmology.* 2012;119:1199–1210.
- Yatsenko AN, Shroyer NF, Lewis RA, Lupski JR. Late-onset Stargardt disease is associated with missense mutations that map outside known functional regions of ABCR (ABCA4). *Hum Genet.* 2001;108:346–355.
- Chen L, Lee W, de Carvalho JRL, et al. Multi-platform imaging in ABCA4-associated disease. *Sci Rep.* 2019;9:6436.
- Duncker T, Marsiglia M, Lee W, et al. Correlations among near-infrared and short-wavelength autofluorescence and spectral-domain optical coherence tomography in recessive Stargardt disease. *Invest Ophthalmol Vis Sci.* 2014;55:8134–8143.
- Jauregui R, Park KS, Duong JK, Mahajan VB, Tsang SH. Quantitative progression of retinitis pigmentosa by optical coherence tomography angiography. *Sci Rep.* 2018;8:13130.
- Mastropasqua R, Toto L, Borrelli E, et al. Optical coherence tomography angiography findings in Stargardt disease. *PLoS One.* 2017;12:e0170343.
- Battaglia Parodi M, Cicinelli MV, Rabiolo A, Pierro L, Bognesi G, Bandello F. Vascular abnormalities in patients with Stargardt disease assessed with optical coherence tomography angiography. *Br J Ophthalmol.* 2017;101:780–785.
- de Carlo TE, Adhi M, Salz DA, et al. Analysis of choroidal and retinal vasculature in inherited retinal degenerations using optical coherence tomography angiography. *Ophthalmic Surg Lasers Imaging Retina.* 2016;47:120–127.
- Battaglia Parodi M, Arrigo A, MacLaren RE, et al. Vascular alterations revealed with optical coherence tomography angiography in patients with choroideremia. *Retina.* 2019;39:1200–1205.
- Al-Sheikh M, Falavarjani KG, Pfau M, Uji A, Le PP, Sadda SR. Quantitative features of the choriocapillaris in healthy individuals using swept-source optical coherence tomography angiography. *Ophthalmic Surg Lasers Imaging Retina.* 2017;48:623–631.
- Spaide RF, Fujimoto JG, Waheed NK, Sadda SR, Staurengi G. Optical coherence tomography angiography. *Prog Retin Eye Res.* 2018;64:1–55.
- Spaide RF, Klancnik JM, Cooney MJ. Retinal vascular layers imaged by fluorescein angiography and optical coherence tomography angiography. *JAMA Ophthalmol.* 2015;133:45–50.
- Wolock CJ, Stong N, Ma CJ, et al. A case-control collapsing analysis identifies retinal dystrophy genes associated with ophthalmic disease in patients with no pathogenic ABCA4 variants. *Genet Med.* 2019;21:2336–2344.
- Schneider CA, Rasband WS, Eliceiri KW. NIH image to ImageJ: 25 years of image analysis. *Nat Methods.* 2012;9:671–675.
- Zhang Y, Harrison JM, Nateras OS, Chalfin S, Duong TQ. Decreased retinal-choroidal blood flow in retinitis pigmentosa as measured by MRI. *Doc Ophthalmol.* 2013;126:187–197.
- Falsini B, Anselmi GM, Marangoni D, et al. Subfoveal choroidal blood flow and central retinal function in retinitis pigmentosa. *Invest Ophthalmol Vis Sci.* 2011;52:1064–1069.
- Giani A, Pellegrini M, Carini E, Peroglio Deiro A, Bottoni F, Staurengi G. The dark atrophy with indocyanine green angiography in Stargardt disease. *Invest Ophthalmol Vis Sci.* 2012;53:3999–4004.
- Adhi M, Read SP, Ferrara D, Weber M, Duker JS, Waheed NK. Morphology and vascular layers of the choroid in Stargardt disease analyzed using spectral-domain optical coherence tomography. *Am J Ophthalmol.* 2015;160:1276–1284.e1.
- Battaglia Parodi M, Cicinelli MV, Rabiolo A, et al. Vessel density analysis in patients with retinitis pigmentosa by means of optical coherence tomography angiography. *Br J Ophthalmol.* 2017;101:428–432.
- Sparrow JR, Wu Y, Kim CY, Zhou J. Phospholipid meets all-trans-retinal: the making of RPE bisretinoids. *J Lipid Res.* 2010;51:247–261.
- Burke TR, Duncker T, Woods RL, et al. Quantitative fundus autofluorescence in recessive Stargardt disease. *Invest Ophthalmol Vis Sci.* 2014;55:2841–2852.
- Genead MA, Fishman GA, Stone EM, Allikmets R. The natural history of Stargardt disease with specific sequence mutation in the ABCA4 gene. *Invest Ophthalmol Vis Sci.* 2009;50:5867–5871.
- Cella W, Greenstein VC, Zernant-Rajang J, et al. G1961E mutant allele in the Stargardt disease gene ABCA4 causes bull's eye maculopathy. *Exp Eye Res.* 2009;89:16–24.
- Burke TR, Fishman GA, Zernant J, et al. Retinal phenotypes in patients homozygous for the G1961E mutation in the ABCA4 gene. *Invest Ophthalmol Vis Sci.* 2012;53:4458–4467.
- Kurihara T, Westenskow PD, Gantner ML, et al. Hypoxia-induced metabolic stress in retinal pigment epithelial cells is sufficient to induce photoreceptor degeneration. *Elife.* 2016;5:e14319.
- Marneros AG, Fan J, Yokoyama Y, et al. Vascular endothelial growth factor expression in the retinal pigment epithelium is essential for choriocapillaris development and visual function. *Am J Pathol.* 2005;167:1451–1459.
- Keilhauer CN, Delori FC. Near-infrared autofluorescence imaging of the fundus: visualization of ocular melanin. *Invest Ophthalmol Vis Sci.* 2006;47:3556–3564.
- Greenstein VC, Schuman AD, Lee W, et al. Near-infrared autofluorescence: its relationship to short-wavelength autofluorescence and optical coherence tomography in

- recessive Stargardt disease. *Invest Ophthalmol Vis Sci.* 2015;56:3226–3234.
35. Sampson DM, Gong P, An D, et al. Axial length variation impacts on superficial retinal vessel density and foveal avascular zone area measurements using optical coherence tomography angiography. *Invest Ophthalmol Vis Sci.* 2017;58:3065–3072.
36. Linderman R, Salmon AE, Strampe M, Russillo M, Khan J, Carroll J. Assessing the accuracy of foveal avascular zone measurements using optical coherence tomography angiography: segmentation and scaling. *Transl Vis Sci Technol.* 2017;6(3):16.
37. Llanas S, Linderman RE, Chen FK, Carroll J. Assessing the use of incorrectly scaled optical coherence tomography angiography images in peer-reviewed studies: a systematic review. *JAMA Ophthalmol.* 2019;138:86–94.